doi: 10.15407/ujpe61.09.0806

M.B. DREVAL,[1] O.V. TURIANSKA [2]

[1] National Science Center "Kharkov Institute of Physics and Technology", Nat. Acad. of Sci. of Ukraine
(1, Akademichna Str., Kahrkiv 61108, Ukraine)
[2] V.N. Karazin Kharkiv National University
(4, Svobody Sq., Kharkiv 61022, Ukraine)

CONCERNING SPACE DISTRIBUTION OF THE SOFT X-RAY EMISSIVITY IN THE U-3M TORSATRON

PACS 52.55.Hc; 52.70.La

A miniature pinhole camera array has been installed on the U-3M torsatron for spatially resolved measurements of soft X-ray plasma emission along 20 lines of sights. The recent line-integrated SXR emission data provide important information about the U-3M plasma confinement. The local SXR emissivity distribution in the poloidal cross-section "A-A" is calculated numerically on the base of experimental data. The U-3M magnetic surfaces have been approximated as a set of normalized plasma radius data in the grid covering this cross-section. The local SXR emissivity is determined as a function of the normalized radius. The line-integrated SXR emission is calculated for every viewing area of each SXR channel on the base of this local emissivity in the real geometry of the SXR diagnostics. A fitting of the calculated line-integrated SXR emission profiles to the experimental profiles shows that the radial profiles of local SXR emissivity are quite narrow, with strong gradient in the central plasma part. The SXR emissivity profiles are quite different from the parabolic form.

K e y w o r d s: U-3M, SXR, tomography.

1. Introduction

Soft X-ray (SXR) diagnostics is an important tool for the study of various phenomena in tokamaks, stellarators, reverse field pinches, *etc.* An advantage of the SXR diagnostics is a possibility of multichannel plasma profile evolution measurements with excellent temporal and spatial resolutions. Nonetheless, the SXR signal dependence on a set of parameters and its integral character form difficulties in the SXR data interpretation. Under the assumption of the bremsstrahlung radiation from a Maxwellian plasma, the SXR emission at a detector depends on a combination of the electron density n_e, temperature T_e, and effective plasma charge Z_{eff}. In the case of 2 μm Al foil filter, used in U-3M SXR diagnostics, the impact of the local SXR emissivity to the detector signal is proportional to $g \propto T_e n_e^2 Z_{\text{eff}}^2$ [1,2]. Under the assumption of uniform Z_{eff}, we can roughly estimate the electron density and temperature profiles shapes. For example, if both of them are flat, the SXR emissivity profile cannot be peaked. The amount of a diagnostics installed on the U-3M is limited. In such a situation, a SXR diagnostics is one of the few diagnostics available for plasma profile measurements [3]. It is unique in the U-3M diagnostics, by allowing one to study the main plasma profile with the use of single discharge data (also available H_α profile is not directly related to the plasma core). The plasma profile behavior during the so-called H-like mode transition [4, 5] is one of the U-3M questions without an answer up to now. The expected plasma

confinement improvement will cause the plasma temperature or density to rise (or both of them), which will cause a substantial rise of the SXR emission. A transport barrier can be localized by the SXR emission profile gradient steepening. The local SXR emissivity profile is required for the plasma confinement analysis. In order to reconstruct a local emissivity profile on the base of single SXR array data, the assumption that the SXR emissivity g is a function of the magnetic surfaces $g = g(\rho)$ should be used, where ρ is the normalized plasma radius. In this case, we can simplify the two-dimensional problem to a one-dimensional one and use a single SXR array. In the presence of an electron beam, for example, this assumption is not valid, thus, our framework is limited. Our assumption is valid for the U-3M discharges with moderate plasma density, where no suprathermal electrons are observed, and needs the additional consideration for low-density discharges, where the evidence of suprathermal electrons was demonstrated by the ECE diagnostics [6]. Fluctuations of the SXR emission observed in U-3M [3] form another exception from the framework under consideration. In order to obtain the local emissivity g, the tomographic inverse problem should be solved (see Refs. [7–9] and references therein). The tomographic inversion is widely used in stellarators (e.g., W-7AS [10, 11], TJ-II [12], LHD [13, 14], H-1 [16], WEGA [15]) and tokamaks (e.g., TCV [9], JET [8], Tore Supra [17], COMPASS [18]). Mathematically, the problem consists of solving the system of integral equations $f_j = \int_{S_j} g ds$; $j = 1, ..., n_j$, where the integral is taken along the line of sight, and n_j is the number of available measurements. This equation can represent an underdetermined (if the number of measurements j is less than the number of space zones of reconstruction) or overdetermined system. In tomography, the function $g(\mathbf{r})$ is approximated by the expansion in a suitable set of basis functions $b_j(\mathbf{r})$: $g \approx \sum_j g_j b_j(\mathbf{r})$ with expansion coefficients g_j. If a substantial amount (substantial number of SXR lines of sight) of linearly independent (more than one SXR detector array) measurements are available, then the 2-D ($b_j(x, y)$) or even 3-D ($b_j(x, y, z)$) tomography can be used. The 2-D tomography is recently used in the modern fusion devices [8,9]. In the 2-D case, the local basis functions (square pixels, pixels in a form of sections of rings that match the flux surfaces, *etc.*) including natural basis functions (based on the functional shape of the viewing geometry) and global basis functions (like in the Mac-Cormack method based on the Zernike polynomials) were used [7, 8]. The square pixel basis functions were used in recent works [9, 17] as an universal one due to a rather complex topology of magnetic surfaces and due to 3-5 SXR arrays available in these devices. This type of the inversion is also caused by the fact that, in most of modern fusion devices, the radial distributions of quasistationary plasma parameters (like n_e and T_e) are measured directly, and the SXR emissivity is used in the investigations of transient non-stationary phenomena only. In addition to the transient plasma behavior investigation, the SXR arrays viewing toroidally were used recently in fusion devices [13, 14]. In the overdetermined case, the least-squares fit algorithm provides a sufficient accuracy of the inversion [8, 9]. In the underdetermined case, additional constraints on the function g are represented by the regularization technique. The linear regularization, maximum entropy, and minimum Fisher regularization (MFR) methods have been widely used [8,9]. The pixel-style is, in general, a rather unsatisfactory choice for many situations, because it employs none of the additional information that one has *a priori*, for example, about various approximate symmetries. In the stationary equilibrium case, the SXR emissivity, as discussed above, is a function of the magnetic surface $g = g(\rho)$. We can reduce the number of degrees of freedom owing this information and convert our problem to the 1-D case ($b_j(x, y) = b_j(\rho(x, y)) = b_j(\rho)$). Due to only one SXR array of 20 channels available in the U-3M torsatron, we should use this tomographic technique. On the other hand (as a remark), for non-stationary periodic processes, the simple tomographic technique based on a 1-D Singular Value Decomposition (SVD) [19] provides a sufficient accuracy, and even single array can be used, if the symmetry of the magnetic surfaces is taken into account. In the case of 1-D conversion, the underdetermined system of integral equations is thus transformed into an overdetermined system of algebraic equations for the coefficients of the base functions, which can be solved, by using a least-squares fit. Such a solution is provided, for example, by the Mac-Cormack–Granetz algorithm [8, 9], which is widely used in fusion researches. Since the Abel inversion technique [7, 8], the 1-D tomographic technique was used in old fusion experiments [7, 8] and still used recently in [11, 12, 16].

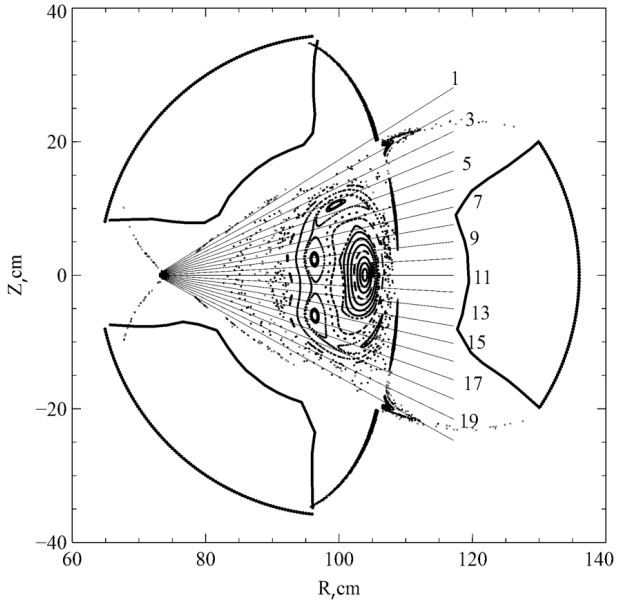

Fig. 1. Magnetic surfaces, divertor fluxes, and central lines of sight of the SXR detector array across the U-3M cross section "A-A"

In our work, we do not pretend on the quite accurate tomographic inversion. In the experimentally observed up-down asymmetry of the line-integrated SXR emission profile caused by misalignments of the SXR diagnostics [1, 3], the difference between local profiles reconstructed with the use of the up or down part of the experimental profiles exceeds the possible errors in calculations.

2. SXR Diagnostics Setup and Experimental Data

The 2 μm Al foil has been installed in the U-3M SXR pinhole diagnostics [1] to cut-off the low-energy radiation. The SXR camera array consists of a 20-channel photodiode linear array IRD AXUV-20EL. The camera is viewing horizontally through a symmetric plasma cross-section "A-A", as is shown in Fig. 1. The gain of SXR photodiode photocurrent amplifiers is 2.5×10^7 V/A. The bandwidth of amplifiers is 10 kHz. It allows one to suppress successfully the high-level RF noise and to register SXR signals [1]. An example of the SXR profile temporal behavior in a low-density frame antenna discharge with the transition at 37.5 ms is shown in Fig. 2 [3]. The transition is related to the complex U-3M plasma column perturbation associated with the MHD activity [3]. No smoothing is applied to the data in Fig. 2, *b* in order to demonstrate the accuracy of the SXR emission profile measurement, in contrast to Fig. 2, *a*, where the spatial interpolation of the data from 20 channels and the temporal averaging are used. As is seen from Fig. 2, *b*, the major source of the SXR emissivity measurement error is based on the profile asymmetry due to the SXR diagnostics misalignment. The space derivative irregularity of the profile can be determined by the 5–10% accuracy of the relative sensitivity of the SXR channels (due to the geometrical design and electronics of the SXR diagnostics), as well as due to some impact of the non-equilibrium SXR emission due to plasma fluctuations. We should note that, according to the statistical comparison of the SXR emissivity in a set of similar U-3M discharges, the accuracy of a equilibrium SXR profile averaged over the time is 5–7%.

An example of the SXR profile modification on the final degradation stage of the three half-turn antenna discharge is shown in Fig. 3 [3]. A peaking of the SXR emission profile near the discharge end is clearly seen even by the line-integrated SXR data. This indicates that the plasma cooling at a periphery occurs. Probably, a degradation of the RF power absorption at the periphery appears at the end of the THT antenna discharge under consideration.

3. Calculation of the Local SXR Emissivity

In order to the calculate line-integrated data with the use of a single SXR array, the distribution of the SXR emissivity across the polidal cross section $g(R, z)$ is assumed to be a function of the normalized plasma radius ρ as $g(\rho(R, z))$, where R is the major plasma radius, and z is the vertical coordinate. The topology of U-3M magnetic surfaces is quite complex, as it is shown in Figs. 1 and 4, *a*. We need to construct the monotonic function $\rho(R_i, z_j)$ at the grid points R_i and z_j from a set of unsorted data supplied by the code of calculations of U-3M magnetic surfaces provided by Dr. Nemov [20]. The chains of magnetic islands form additional difficulties. In our calculations, the value of normalized radius inside magnetic islands is assumed to be equal to its value in the outer border of islands. In the region outside of the confinement area (where minor radius is $a > 12$ cm, and normalized radius $\rho > 1$),

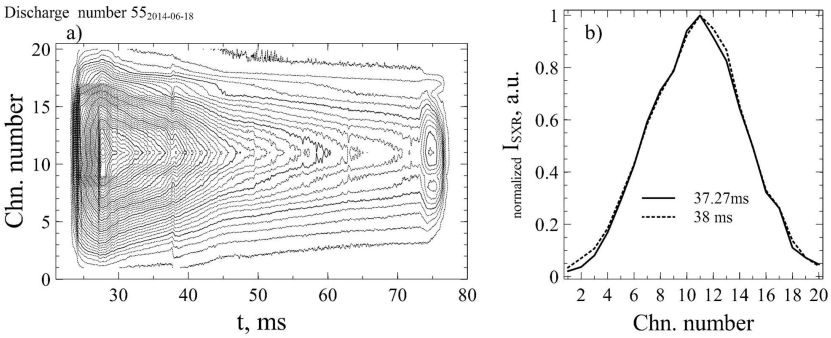

Fig. 2. SXR profile in a low-density discharge (a). Distribution of the SXR emission before (at 37.27 ms) and after (at 38 ms) the transition (b)

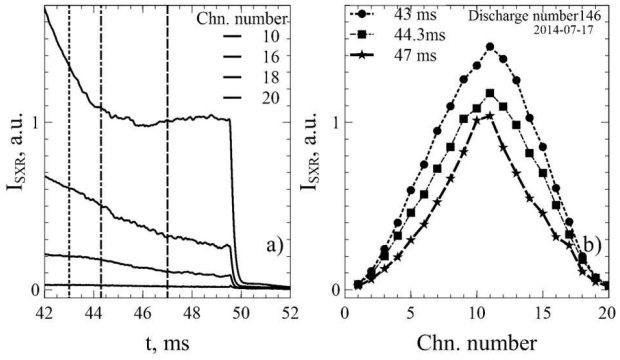

Fig. 3. SXR profile at the end of a THT discharge

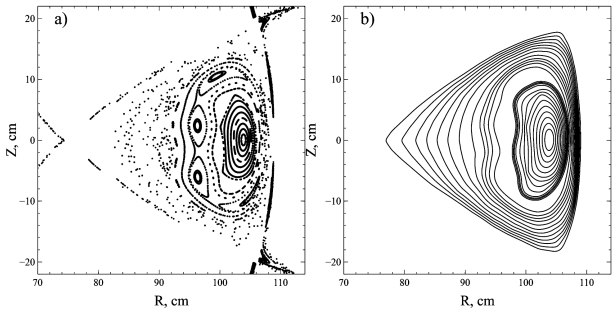

Fig. 4. Magnetic surfaces and divertor fluxes (a); $\rho(R, z)$ contour-lines (b). U-3M cross section "A-A"

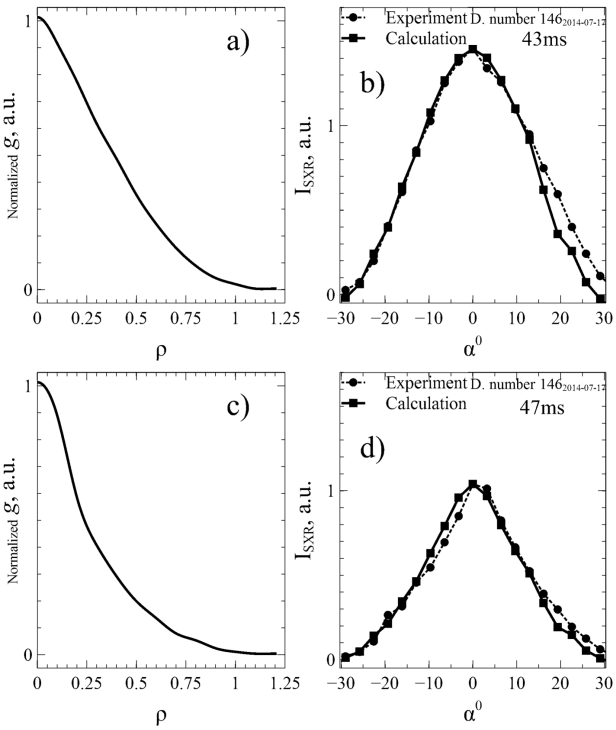

Fig. 5. Local SXR emissivity profiles g and calculated line integrated SXR emission profiles I_{SXR} for two time moments

the unclosed magnetic surfaces (sets of drifted radially points) were approximated as some surfaces with constant normalized radius in order to use this area in our calculation. The $\rho(R_i, z_j)$ function was smoothed numerically by the moving average in order to remove jumps of its derivative. The function $\rho(R, z)$ constructed under these assumptions is shown in Fig. 4, *b*. Calculations of the line integrated SXR signal were performed in the real geometry of the SXR diagnostics in the U-3M. The line-integrated SXR signal for each of the SXR channel was calculated using the set of 10 lines in order to take the poloidal divergence of its viewing area into account [1]. It was calculated, by using the numerical integration of the input local emissivity profile $g(\rho)$ and the $\rho(R, z)$ data. The local emissivity distribution profile $g(\rho)$ was varied by the values of 13 base points with the spline connection between these points. The spline style of the

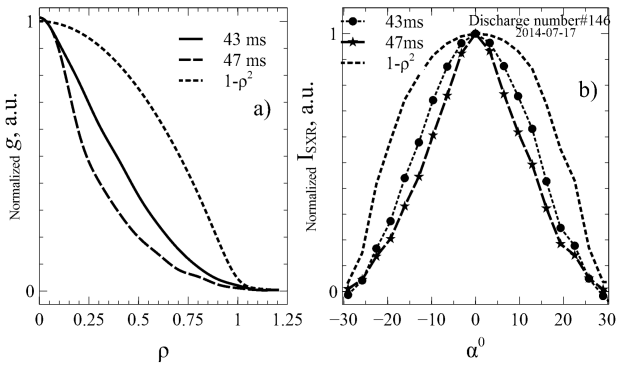

Fig. 6. Local SXR emissivity profiles g at 43 ms and 47 ms of the discharge $146_{2014-07-17}$ and a parabolic profile; calculated line-integrated $I_{\rm sxr}$ profiles

connection of base points determines the smoothness constrain to the emissivity g, as well as 13 points per plasma radius constrains the type of this function. We used the least-squares fit algorithm in calculations. The results of calculations at 43 ms and 47 ms of the discharge $146_{2014-07-17}$ are shown in Fig. 5.

The significant up-down asymmetry of the experimental profiles is clearly observed in Fig. 5 and causes the discrepancy of the fitting of up-side and down-side profiles. The asymmetry is caused by misalignments of the SXR diagnostics and, in particular, by some angle between the SXR viewing plane and the poloidal cross-section "A-A". The toroidal declination of the viewing plane leads to a modification of the shape of viewing magnetic surfaces. It can cause the observed asymmetry and cause uncertainties in the local emissivity profile determination. In addition, a possible discrepancy between calculated and real magnetic surfaces can cause an additional asymmetry. Nonetheless, the profile modifications induced by the plasma behavior substantially overcome those uncertainties, as it is clear, for example, from Fig. 5. Figure 6 summarizes the calculations and compares the U-3M SXR emissivity profiles with a parabolic profile.

Our calculations clearly show the strong peaking of the emissivity profile. This peaking is observed in most of the U-3M discharges with sufficiently hot plasma (where the measurable SXR emission is present). This result is in a qualitative agreement with the narrow profile of the emissivity of the C_V spectral line [21]. This indicates that the U-3M electron density and temperature profiles are quite narrow, in contrast to the profiles usually observed in stellarator-like fusion devices (e.g., in LHD [22], CHS [23], and TJ-II [24]).

4. Summary and Conclusions

The local SXR emissivity distribution in the poloidal cross-section "A-A" is calculated numerically on the base of experimental data. The U-3M magnetic surfaces have been approximated as a set of normalized plasma radius data in the grid covering this cross-section. The local SXR emissivity is determined as a function of the normalized radius. The line-integrated SXR emission is calculated for every viewing area of each SXR channel on the base of this local emissivity in the real geometry of the SXR diagnostics. A fitting of the calculated line-integrated SXR emission profiles to the experimental profiles shows that the radial profiles of local SXR emissivity are quite narrow with strong gradient in the central plasma part.

1. M.B. Dreval, Design and initial operation of multichord soft X-ray detection array on the U-3M torsatron, *Probl. Atom. Sci. Technol.* **6(20)**, 250 (2014); available at `http://vant.kipt.kharkov.ua/ARTICLE/VANT_2014_6/article_2014_6_250.pdf`.
2. M.B. Dreval, Design of multichord soft X-ray detection arrays for the Uragan-2M stellarator, *Probl. Atom. Sci. Technol.* **6**, 11 (2010); available at `http://vant.kipt.kharkov.ua/ARTICLE/VANT_2010_6/article_2010_6_11.pdf`.
3. M.B. Dreval, First results of multichord soft X-ray detection array on the U-3M torsatron, *Probl. Atom. Sci. Technol.* **1**(95), 8 (2015); available at `http://vant.kipt.kharkov.ua/ARTICLE/VANT_2015_1/article_2015_1_8.pdf`.
4. V.V. Chechkin, I.M. Pankratov, L.I. Grigor'eva *et al.*, RF discharge dynamics with passing over L- and H-like mode states in the Uragan-3M torsatron, *Probl. Atom. Sci. Technol.* **6**(82), 3 (2012); available at `http://vant.kipt.kharkov.ua/ARTICLE/VANT_2012_6/article_2012_6_3.pdf`.
5. I.M. Pankratov, A.A. Beletskii, V.L. Berezhnyj *et al.*, Behavior of RF discharge plasmas in the Uragan-3M and Uragan-2M torsatrons, *Contrib. Plasma Phys.* **50**, 520 (2010) [DOI: 10.1002/ctpp.200900012].
6. R.O. Pavlichenko, Influence of suprathermal electrons on ECE measurements in the Uragan-3M torsatron, *Probl. Atom. Sci. Technol.* **1**(95), 293 (2015); available at `http://vant.kipt.kharkov.ua/ARTICLE/VANT_2015_1/article_2015_1_293.pdf`.

7. V. Pickalov and N. Preobrazhenski, *Reconstructive Tomography in Gas Dymanics and Plasma Physics* (Nauka, Novosibirsk, 1987) (in Russian).
8. L.C. Ingesson, B. Alper, B.J. Peterson, and J.-C. Vallet, Chapter 7: Tomography diagnostics: bolometry and soft-X-ray detection, *Fusion Science and Technology*, **53**, 528 (2008) [DOI: 10.13182/FST53-528].
9. M. Anton, H. Weisen, M.J. Dutch *et al.*, X-ray tomography on the TCV tokamak, *Plasma Phys. Control. Fusion*, **38**, 1849 (1996) [DOI: 10.1088/0741-3335/38/11/001].
10. K. Ertl, W. von der Linden, V. Dose, and A. Weller, Maximum entropy based reconstruction of soft X-ray emissivity profiles in W7-AS, *Nucl. Fusion* **36**, 1477 (1996) [DOI: 10.1088/0029-5515/36/11/I03].
11. A.P. Navarro, M.A. Ochando, and A. Weller, Equilibrium-based iterative tomography technique for soft X-ray in stellarators, *IEEE Transactions on Plasma Science* **19**, 569 (1991) [DOI: 10.1109/27.90321].
12. A.P. Navarro, V.K. Paré, and J.L. Dunlap, Two-dimensional spatial distribution of volume emission from line integral data, *Rev. Sci. Instrum.* **52**, 1634 (1981) [DOI: 10.1063/1.1136510].
13. S. Ohdachi, K. Toi, G. Fuchs, S. von Goeler, and S. Yamamoto, High-speed tangentially viewing soft X-ray camera to study magnetohydrodynamic fluctuations in toroidally confined plasmas, *Rev. Sci. Instrum.* **74**, 2136 (2003) [DOI: 10.1063/1.1537449].
14. R. Sano, B.J. Peterson, M. Kobayashi *et al.*, Reconstruction of 3-D radiation profile from 2-D images viewed by IR imaging video bolometers with SVD, *IEEE Trans. on Plasma Sci.* **42**, 2860 (2014) [DOI: 10.1109/TPS.2014.2330605].
15. D. Zhang, M. Glaubitz, H.P. Laqua *et al.*, Determination of electron thermal diffusivity at the WEGA stellarator, *Nucl. Fusion* **52**, 043002 (2012) [DOI: 10.1088/0029-5515/52/4/043002].
16. S. Ma, J. Howard, B.D. Blackwell, and N. Thapar, Measurements of electron density and temperature in the H-1 heliac plasma by helium line intensity ratios, *Rev. Sci. Instrum.* **83**, 033102 (2012) [DOI: 10.1063/1.3692756].
17. D. Mazon, D. Vezinet, D. Pacella *et al.*, Soft X-ray tomography for real-time applications: present status at Tore Supra and possible future developments, *Rev. Sci. Instrum.* **83**, 063505 (2012) [DOI: 10.1063/1.4730044].
18. M. Odstrčil, J. Mlynář, V. Weinzettl *et al.*, Plasma tomographic reconstruction from tangentially viewing camera with background subtraction, *Rev. Sci. Instrum.* **85**, 013509 (2014) [DOI: 10.1063/1.4862652].
19. C. Nardone, Multichannel fluctuation data analysis by the singular value decomposition method. Application to MHD modes in JET, *Plasma Phys. Control. Fusion*, **34**, 1447 (1992) [DOI: 10.1088/0741-3335/34/9/001].
20. V.N. Kalyuzhnyj and V.V. Nemov, Calculations of $1/\nu$ Transport in an $l = 3$ stellarator magnetic field in the presence of magnetic islands caused by magnetic system errors, *Fusion Sci. Technol.* **46**, 248 (2004); available at `http://www.ans.org/pubs/journals/fst/a_562`.
21. V.N. Bondarenko, V.G. Konovalov, S.A. Tsybenko, V.S. Voitsenya, and E.D. Volkov, Investigation of radial distributions of spectral line radiation emissivities in torsatron "Uragan-3M", *Probl. Atom. Sci. Technol.* **1**(9), 23 (2003); available at `http://vant.kipt.kharkov.ua/ARTICLE/VANT_2003_1/article_2003_1_23.pdf`.
22. M. Fujiwara, K. Kawahata, N. Ohyabu *et al.*, Overview of LHD experiments, *Nucl. Fusion* **41**, 1355 (2001) [DOI: 10.1088/0029-5515/41/10/305].
23. A. Fujisawa, H. Iguchi, T. Minami *et al.*, Experimental study of the bifurcation nature of the electrostatic potential of a toroidal helical plasma, *Phys. Plasmas* **7**, 4152 (2000) [DOI: 10.1063/1.1290483].
24. J. Sánchez, D. Alegre, A. Alonso *et al.*, Transport, stability and plasma control studies in the TJ-II stellarator, *Nucl. Fusion* **55**, 104014 (2015) [DOI: 10.1088/0029-5515/55/10/104014].

Received 07.05.16

М.Б. Древаль, О.В. Турянська

СТОСОВНО ПИТАННЯ
ПРО ПРОСТОРОВИЙ РОЗПОДІЛ ЕМІСІЇ
М'ЯКОГО РЕНТГЕНА В ТОРСАТРОНІ У-3М

Р е з ю м е

Мініатюрний датчик для вимірювання просторового розподілу випромінювання м'якого рентгена уздовж двадцяти хорд був встановлений на торсатроні У-3М. Нещодавно отримана еволюція профілю інтегрального випромінювання м'якого рентгена у розряді У-3М дає важливу інформацію щодо утримання плазми торсатрона У-3М. У даній роботі шляхом чисельних розрахунків знайдено розподіл локальної емісії м'якого рентгена по перерізу "А-А" торсатрона У-3М, базуючись на експериментальних даних. Виконано апроксимацію магнітних поверхонь перерізу "А-А" у вигляді набору значень величини нормованого радіуса у вузлах сітки, яка покриває даний переріз. У реальній геометрії комплексу діагностики м'якого рентгенівського випромінювання на У-3М виконано чисельне знаходження розподілу інтегрального випромінювання на кожному з двадцяти діагностичних каналів для різних модельних профілів емісії і порівняно їх з експериментом.